Earth Surf. Dynam. Discuss., doi:10.5194/esurf-2016-56, 2016
Manuscript under review for journal Earth Surf. Dynam.
Published: 25 November 2016

Earth Surface Dynamics Discussions
Open Access
EGU

Self-similar growth of a bimodal laboratory fan

Pauline Delorme[1], Vaughan Voller[2], Chris Paola[2], Olivier Devauchelle[1], Éric Lajeunesse[1], Laurie Barrier[1], and François Métivier[1]

[1]Institut de Physique du Globe de Paris, Paris - Sorbonne Paris Cité, Université Paris Diderot, Paris, France
[2]Saint Anthony Falls Laboratory, University of Minnesota, Minneapolis, Minnesota, USA

Correspondence to: P. Delorme (pdelorme@ipgp.fr)

Abstract. Using laboratory experiments, we investigate the growth of an alluvial fan fed with two distinct granular materials. Throughout the growth of the fan, its surface maintains a radial segregation, with the less mobile sediment concentrated near the apex. Scanning the fan surface with a laser, we find that the transition between the proximal and distal deposits coincides with a distinct slope break. A radial cross-section reveals that the stratigraphy of the deposit bears the mark of this consistent segregation. To interpret these observations, we conceptualize the fan as a radially symmetric structure that maintains its geometry as it grows. When combined with slope measurements, this model proves consistent with the sediment mass balance and successfully predicts the slope of the proximal-distal transition as preserved in the fan stratigraphy. The threshold channel theory provides an order-of-magnitude estimate of the fan slope, but relatively high sediment discharges manifest themselves in the form of slopes 3-5 times higher than those predicted from the theory.

1 Introduction

When it leaves a mountain range to enter lowlands, a river hits shallow slopes and loses valley confinement. This abrupt change causes it to deposit its sedimentary load into an alluvial fan (Bull, 1977; Rachocki and Church, 1990; Blair and McPherson, 1994; Harvey et al., 2005). As the river builds this sedimentary structure, its bed rises above the surrounding land, and its channel becomes unstable. At this point, either the river erodes its banks to migrate laterally, or it overflows them during a catastrophic flood event, called "avulsion" (Slingerland and Smith, 2004; Sinha, 2009). In both cases, the river constantly explores new paths to fill up hollows in the deposit surface and preserve its radial symmetry. The resulting deposit acquires the conical shape which characterizes alluvial fans.

As the first sedimentary archive along the river's course, an alluvial fan records the history of its catchment (Hinderer, 2012). Indeed, the geometrical reconstruction of a fan provides an estimate of its volume which, through mass balance, yields the average denudation rate of the catchment (Kiefer et al., 1997; Jayko, 2005; Jolivet et al., 2014; Guerit et al., 2016). Furthermore, when the river transports multiple grain sizes, it usually deposits the coarser sediment near the fan apex, and the finer sediment at its toe. This segregation produces a gravel front which moves forward and backward as the fan adjusts to external forcing. In radial cross-section, this series of progradations and retrogradations appears as a boundary between lithostratigraphic units, a pattern often interpreted as the signature of tectonic or climatic events (Paola et al., 1992a; Clevis et al., 2003; Charreau et al., 2009; Whittaker et al., 2011; Dubille and Lavé, 2015).

Earth Surf. Dynam. Discuss., doi:10.5194/esurf-2016-56, 2016
Manuscript under review for journal Earth Surf. Dynam.
Published: 25 November 2016

To interpret the morphology and stratigraphy of an alluvial fan, we need to understand how it translates the input signal (e.g., water and sediment discharges) into its own geometry (e.g., its size, downstream slope and stratigraphy). For instance, Drew (1873) observed that the lower the water discharge Q_w, the steeper the fan slope. More recent observations point at the influence of the sediment discharges Q_s on the slope, often in the form of the ratio Q_s/Q_w (Parker et al., 1998 a, b). The slope steepens according to the increase of this ratio. At first sight, the shape of an alluvial fan is well approximated by a perfect cone, but a closer look often reveals a steeper slope near the apex. Possible explanations for this curvature include the decrease in sediment discharge caused by deposition, and the downstream fining of the sediment grain (Blissenbach, 1952; Rice, 1999; Stock et al., 2008; Miller et al., 2014).

Only seldom do field measurements allow us to separate the various parameters affecting the morphology of a fan, making it difficult to isolate their respective influence. One way around this problem is to use laboratory experiments, where small alluvial fans can be easily produced (Schumm et al., 1987; Parker, 1999; Paola et al., 2009; Clarke, 2015). When water and sediment are injected onto the bottom of a tank, a deposit spontaneously forms around its inlet. The formation of this deposit is remarkably similar to that of natural fans: small rivers distribute the sediment across its surface, and migrate laterally to maintain its radial symmetry. As the forcing parameters vary, the deposit responds by adjusting its morphology.

The sediment discharge Q_s determines the growth rate of an experimental fan. Indeed, mass balance requires that the fan volume increase in proportion to the sediment input. As a consequence, the radius of the fan increases as $(Q_s t)^{1/3}$, where t is the time elapsed since the beginning of the experiment (Powell et al., 2012; Reitz and Jerolmack, 2012). Avulsions occur more frequently as the sediment discharge increases, showing that the internal dynamics of an experimental fan adjusts to the forcing (Bryant et al., 1995; Ashworth et al., 2004; Clarke et al., 2010; Reitz and Jerolmack, 2012). This adjustment allows the fan to maintain its conical shape which, at first order and for a single grain size, is simply characterized by its slope.

Even in simplified experiments (constant discharges, single grain size), there is no clear consensus about the mechanism by which a fan selects its own slope. However, most investigators acknowledge that low water discharge, high sediment discharge, and large grains steepen the fan (Le Hooke and Rohrer, 1979). The influence of water and sediment discharge on the slope is often expressed as a growing function of their dimensionless ratio Q_s/Q_w (Whipple et al., 1998; Van Dijk et al., 2009; Powell et al., 2012). At variance with this model, Guerit et al. (2014) propose that all three parameters act independently. In their experiment, the fan grows between two parallel plates that confine it to a vertical plane. Its slope depends essentially on the water discharge and grain size. This observation accords quantitatively with the hypothesis that the flow maintains the deposit surface near the threshold of motion (Glover and Florey, 1951; Parker, 1978; Devauchelle et al., 2011; Seizilles et al., 2013). As for the sediment discharge, it perturbs the fan profile only moderately, by steepening the slope in proportion to its intensity. As the sediment gets deposited, the slope returns to its threshold value, which it reaches at the toe. The curvature thus induced is proportional to the sediment input.

Accordingly, the downstream curvature of an alluvial fan composed of uniform sediment can be interpreted as a signature of spatial variation in sediment transport. What happens when the fan is composed of non-uniform sediment? When the grain size is broadly distributed, downstream fining can also affect the fan profile. This phenomenon occurs in flume experiments, where the larger grains concentrate near the inlet (Paola et al., 1992b; Smith and Ferguson, 1996). In the experiment of Reitz and

Earth Surf. Dynam. Discuss., doi:10.5194/esurf-2016-56, 2016
Manuscript under review for journal Earth Surf. Dynam.
Published: 25 November 2016

Earth Surface Dynamics Discussions Open Access EGU

Jerolmack (2012), the fan builds its upper part out of large grains, and deposit the smaller ones near its toe. Consequently, the proximal slope is significantly steeper than the distal one, a signal whose form is similar to the curvature induced by deposition.

Here, we investigate the impact of a bimodal sediment on the morphology of an alluvial fan. To do so, we generate a laboratory fan fed with a mixture of two granular materials (Sect. 2). Our experiment generates a segregated deposit, similar to the laboratory fan of Reitz and Jerolmack (2012). We first analyze its morphology, describing the growth of each part of the deposit independently (Sect. 3). We then relate the spatial distribution of the sediment to the proximal and distal slopes (Sect.4). Based on these observations, we propose a geometrical model to describe the fan deposit (Sect. 5). Finally, we interpret our observations in the light of the threshold-channel theory (Sect. 6).

2 Experimental set-up

Producing experimental alluvial fans has become routine in geomorphology (Schumm et al., 1987; Clarke, 2015). Here we use a setup similar to that of, for example, Whipple et al. (1998) to generate a radially symmetric fan over a horizontal basal surface (Fig. 1). In our experiments, however, a bimodal sediment mixture allows the fan to a form segregated deposit, visualized by color.

To produce a bimodal sediment, we mix black coal and white silica grains, the colors of which are easily distinguished. The coal grains are larger and lighter than the silica grains (Table 1). To quantify the mobility of these grains, we measure their respective transport laws in independent experiments (Appendix A). We find that, when unmixed, the coal grains are more mobile than the silica grains: For the same shear stress τ, the flux of coal grains is larger than that of silica grains (Fig. 2). When different grains are mixed, however, the shear stress exerted on each type of grains depends on their relative concentration on the bed surface (Wilcock and Crowe, 2003; Houssais and Lajeunesse, 2012). The shear stress required to move large grains is lower than it would in a system of only large grain, because they protrude more into the fluid. Conversely, small grains require a higher shear stress because they are partially shielded from the flow by neighboring larges grains (Einstein, 1950). When the mixture is composed of grains with different densities the exposure/hiding effect is negligible (Viparelli et al., 2015). As a consequence, we now consider that the flow exerts the same shear stress on coal and silica when they are mixed. Accordingly, we use Fig. 2 as a first-order approximation for the differential transport of a mixture of coal and silica. If this interpretation is correct, the experimental river could transport coal while depositing silica, thus segregating the sediments based on their mobility.

Our experimental transport laws feature unambiguous thresholds. Below this critical shear stress τ_c, no sediment is transported. This widespread observation is often interpreted in terms of the critical Shields parameter θ_c, which represents the ratio of the flow-induced shear stress to gravity (Shields, 1936):

$$\theta_c = \frac{\tau_c}{(\rho_s - \rho) g d_s}, \quad (1)$$

where ρ is the density of water, ρ_s is the density of sediment, g is the acceleration of gravity, and we approximate the grain size d_s with its median value d_{50}. For our sediments, the denominator in Eq. (1) is larger for silica than for coal, indicating that

Earth Surf. Dynam. Discuss., doi:10.5194/esurf-2016-56, 2016
Manuscript under review for journal Earth Surf. Dynam.
Published: 25 November 2016

the density difference prevails over grain size to govern the mobility of our grains. In addition, we find the threshold Shields parameter to be about 0.19 for coal, and 0.25 for silica (Table 1), thus reinforcing the mobility contrast.

The tank we use to produce alluvial fans is 2 m-wide, and more than 5 m-long. Its bottom is covered with a black rubber tarpaulin. At the back of the tank, a 30 cm-high, impervious wall simulates the mountain front against which the fan leans; the three other sides are bounded by trenches to evacuate water. At the wall's foot, 5 cm-rocks prevent the flow from concentrating along it. Despite the trenches, surface tension maintains a 0.5 cm-deep sheet of water over the tank bottom.

To ensure constant inputs of water and sediment into the experiment, we use a header tank to supply the water, and an Archimedes screw to supply the grains. The fluxes of water and sediment merge in a funnel, which directs them toward the tank. Before reaching the fan, water and sediment flow through a 10 cm-wide, wire-mesh cylinder filled with pebbles. This device reduces the water velocity and homogenizes the mixture (Fig.1).

An experimental run begins with an empty tank. When the mixture of water and sediment reaches its bottom, it forms a half-cone deposit. Initially, a sheet flow spreads homogeneously over this sediment body. After a few minutes, the flow confines itself into distinct channels (typically five or six), the width of which varies between about 1 and 2 cm. They avulse regularly to maintain the radial symmetry of the fan, much as in the experiments of Bryant et al. (1995) and Reitz and Jerolmack (2012). An experiment stops when the deposit reaches the sides of the tank, typically after 3 to 4 hours.

As it grows, the fan deposits the silica grains upstream of the coal grains. Accordingly, the apex of the fan is composed of silica, whereas coal constitutes most of its toe. The boundary between the two types of sediment follows the path of channels, thus adopting a convoluted shape. At the scale of a channel, silica grains generally concentrate around the thalweg, whereas coal is deposited on the banks. To explore the influence of the sediment composition on the morphology of the fan, we varied ϕ, the proportion of silica in sediment mixture, from 25% to 80% over five experiments (Table 2).

3 Self-similar growth

During each run, we track the evolution of the fan surface with a camera (Nikon D90 with a wide-angle lens Nikon AF DX Fisheye-Nikkor 10.5 mm f/2.8G ED) fixed above the center of the tank. We record an image every minute (Fig. 3a). The exact location of the boundary between silica and coal varies significantly during a run. Eye-averaging over its convolutions, however, suggests a constant ratio between the distance from the boundary to the apex and the total length of the fan. To confirm this observation, we manually locate the fan toe on 26 pictures, 10 minutes apart from each other, during run 2 (Fig. 3a). From these individual measurements, we estimate the average radius R_c of the fan with an accuracy of about 6% on each picture. We then rescale each picture with this value, and average them (Fig. 3b). The resulting picture confirms that the fan is radially symmetric on average, and reveals a somewhat blurred but localized transition between the silica and coal deposits. This observation suggests that the fan preserves the spatial distribution of coal and silica as it grows.

To verify the self-similarity of the fan growth, we analyze the evolution of its geometrical properties during run 2. To do so, we manually locate the silica-coal transition and the fan toe (Fig. 3a). We then calculate the average distance R_s from the apex to the transition. The boundary of the silica deposit being more convoluted than the toe, the precision of R_s is about 19%.

Earth Surf. Dynam. Discuss., doi:10.5194/esurf-2016-56, 2016
Manuscript under review for journal Earth Surf. Dynam.
Published: 25 November 2016

Both distances increase in proportion to the cube root of time (Fig. 4). We interpret this observation as a consequence of mass balance (Powell et al., 2012). Indeed, the total volume V of the fan increases linearly with the duration of the experiment:

$$V \propto Q_s t. \tag{2}$$

In a self-similar fan, any distance scales like the cube root of the fan volume; in particular, both R_c and R_s increase in proportion to $(Q_s t)^{1/3}$. Our observations conform to this scaling, thus supporting the hypothesis of a self-similar fan. Accordingly, the relative location of the transition, defined by the ratio $\mathcal{R} = R_s \,/\, R_c$, remains constant during fan growth ($\mathcal{R} = 0.62 \pm 0.04$ for run 2, Figs.3b and 4).

This self-similarity means that, as it grows, the fan preserves its structure, which can therefore be extrapolated from the final deposit. In the next section, we describe the final deposit, through its slope and radial cross-section.

4 Two imbricated fans

A few minutes after the experiment stops, all the surface water has drained away from the fan, leaving the entire deposit emergent. At this point, we scan the deposit's surface with a laser to measure its topography (OptoEngine MRL-FN-671, 1 W, 671 nm). A line generator converts the beam into a laser sheet (60° opening angle, 1 mm thick), the intersection of which with the fan surface is recorded by a camera attached to the laser, about 2 m above the tank bottom (Sick Ranger E50, 12.5 mm lens). The precision of the measurement is less than 1 mm in every direction.

Using the digital elevation model (DEM) of our experimental fan, we find that the elevation contours are well approximated by concentric circles, another indication of radial symmetry (Fig. 5). This property suggests that we compute the radially-averaged profile of the fan (Reitz and Jerolmack, 2012). To do so, we interpolate the DEM along 34 radii, 5° apart from each other, using the Scipy Ndimage library (Fig. 5). The resulting profiles are similar to each other, and differ from the mean by less than 7% (Fig. 6a). The average fan profile is steeper near the apex than at the toe. When we plot the downstream slope of this average profile as a function of the distance to the apex, the transition appears as a decreasing sigmoid curve (Fig. 6b). To quantify this observation, we fit a hyperbolic tangent to the slope profile. We find that the slope plateaus at about 0.29 near the apex, and at about 0.10 near the toe. The transition between these slopes is a smooth transition with a characteristic length of 32% of the fan length. The exact location of the transition is defined by the inflection point of the fit that occurs at 55% of the fan length (Fig. 6b). The slope thus breaks just where the sediment turns to coal, suggesting that these transitions are closely coupled (Fig. 3, $\mathcal{R} \approx 0.62$).

To evaluate this hypothesis, we now turn our attention to the internal structure of the deposit. After the water and sediment supplies have been switched off, the fan remains cohesive, and we can cut it radially to reveal a vertical cross section (Fig. 7). Silica and coal appear segregated, in accordance with the top-view pictures of the fan (Fig. 3), and with the experiments of Reitz and Jerolmack (2012). Silica concentrates near the apex, in the upper part of the deposit, whereas coal locates at its toe. The transition to coal is complex and somewhat smeared in the stratigraphy. It shows alternate streaks of silica and coal, which extend over about one third of the cross-section area. We interpret the variability in the sand-coal transition in the stratigraphy as the result of channel avulsion.

Earth Surf. Dynam. Discuss., doi:10.5194/esurf-2016-56, 2016
Manuscript under review for journal Earth Surf. Dynam.
Published: 25 November 2016

The surface of the cross-section resembles the average profile of Fig. 6a. Indeed, when superimposed, the two lines become virtually indistinguishable, with the slope break occurring near the transition between silica and coal (Fig. 7). Neglecting the span of the transition, we may approximate the average profile by fitting two straight lines to it. The proximal line joins the apex to the transition (slope 0.29), and the distal line joins the transition to the toe (slope 0.10). The two lines intersect at 56% of the deposit length. Finally, we find that the transition line, which joins this intersection to the origin, passes through the stratigraphic streaks. The transition line thus divides the deposit into two imbricated wedges, with the more mobile sediment lying below the less mobile one. The steady climb of the sand-coal transition in the deposit section reflects the outward growth of the transition accompanied by net deposition. In the next section, we formalize this interpretation in the context of self-similar growth, and combine it with mass balance to understand how the fan builds its deposit.

5 Mass balance

Based on our laboratory observations, we propose a geometrical model of an alluvial fan fed with a bimodal mixture of sediments. We consider a radially symmetric structure, which grows by expanding itself without changing its geometry. A consequence of these assumptions is that the geometry of the fan, at any time, is entirely determined by a fixed, two-dimensional template of its cross section (Fig. 8). The simplest possible template consists of two triangles with a common side. The proximal triangle defines the geometry of the silica deposit, and the distal one represents the coal deposit. Three dimensionless parameters define this template: the proximal slope S_s, the distal slope S_c and the relative location of the transition $\mathcal{R} = R_s/R_c$.

The geometry of the template sets the proportion of silica and coal in the deposit. As a consequence, mass balance relates the three parameters that define the fan template to the composition of the sediment mixture injected in the experiment. Indeed, since the sediment discharge is constant, and assuming the deposit is fully segregated, we should have

$$\frac{V_s}{V_s + V_c} = \phi\,, \tag{3}$$

where V_s is the volume of silica in the deposit, and V_c that of coal. For a self-similar fan, this relationship holds at any time.

The silica deposit is composed of two half-cones sharing their base. Its volume reads

$$V_s = \frac{\pi}{6} R_s^2 H_s\,, \tag{4}$$

where H_s is the elevation of the fan apex. To calculate the volume of coal in the deposit, we first evaluate that of a truncated half cone with slope S_c, radius R_c, and height H_c (the elevation of the transition). We then withdraw the volume of the lower cone of the silica deposit. The resulting volume reads

$$V_c = \frac{\pi}{6} \left(R_c^2 + R_c R_s\right) H_c\,. \tag{5}$$

The proximal and distal slopes are simply those of the corresponding right triangles:

$$S_s = \frac{H_s - H_c}{R_s} \quad \text{and} \quad S_c = \frac{H_c}{R_c - R_s}. \tag{6}$$

Earth Surf. Dynam. Discuss., doi:10.5194/esurf-2016-56, 2016
Manuscript under review for journal Earth Surf. Dynam.
Published: 25 November 2016

Using the four above equations, we finally relate the composition of the sediment mixture to the geometry of the fan, as a function of the slope ratio and the transition location:

$$\phi = \frac{(1-\mathcal{S})\mathcal{R}^4 - \mathcal{S}\mathcal{R}^3 - \mathcal{R}^2}{(\mathcal{R}+1)\left((1-\mathcal{S})\mathcal{R}^3 - 1\right)}, \tag{7}$$

where we have defined the ratio of proximal slope to distal slope $\mathcal{S} = S_s/S_c$. Equivalently we may express the composition of the sediment mixture as a function of the slope ratio and the slope of the transition:

$$\phi = \frac{1-\mathcal{S}_t}{1+\mathcal{S}_t\left((\mathcal{S}\mathcal{S}_t)^2 + 3\mathcal{S}\mathcal{S}_t + 2\right)}, \tag{8}$$

where we have defined the ratio of transition slope to proximal slope $\mathcal{S}_t = S_t/S_s$.

If the template is a reasonable representation of the fan geometry, the location and the slope of the transition and the two slopes of the deposit should adjust to the composition of the sediment input, according to Eqs. (7, 8). To evaluate this model, we measure the geometry of the fan at the end of every experimental run (Table 3). Using the radially averaged profile, we first adjust the proximal and distal slopes and calculate their ratio. Then, we estimate the location of the transition using the position of the inflection point (Sect. 4). We find that the proportion of silica in the deposit, as deduced from our measurements through Eqs. (7, 8), matches the composition of the sediment mixture (Fig. 9).

Despite some imperfections in the experimental set-up and a complex stratigraphy, we find that we can reasonably represent our experimental fan as radially symmetric, fully segregated structure which preserves its shape as it grows. These features determine the dynamics of the fan, and the geometry of its deposit. This model, however, involves two free parameters: the proximal and distal slopes. These are selected by the fan itself, by a mechanism that remains to be understood. The next section addresses this problem.

6 Fan slope

Two imbricated deposits make up our experimental fan. Each deposit is built by a collection of channels, which select their own slope according to the type of sediment they flow onto, and to their sediment and water discharges. The deposit then inherits the slope of the channels that build it.

The way a river selects its morphology is still a matter of debate, but it has been recently pointed out that most laboratory rivers, including those flowing over an experimental fan, compare well with the threshold-channel theory (Reitz and Jerolmack, 2012; Seizilles et al., 2013; Reitz et al., 2014; Métivier et al., 2016b). The experiments of Stebbings (1963) suggest that sediment discharge causes a channel to widen, until it becomes unstable and breaks into a braid (Métivier et al., 2016b). The individual threads of a braid, in their turn, behave as threshold channels, both in laboratory flumes and in natural rivers (Reitz et al., 2014; Gaurav et al., 2015; Métivier et al., 2016a).

Returning to our experimental fans, we find them enmeshed in a collection of channels flowing radially (Fig. 10). These channels sometimes ramify downstream, but do not recombine as they would in a braided river. However, following the above contributions, we would like to compare their slope to the threshold-channel theory. Unfortunately, our experimental setup

Earth Surf. Dynam. Discuss., doi:10.5194/esurf-2016-56, 2016
Manuscript under review for journal Earth Surf. Dynam.
Published: 25 November 2016

Earth Surface Dynamics Discussions Open Access EGU

does not allow us to measure their individual water discharges. If the water flow distributes itself evenly among the channels, though, we can approximate their individual discharges to a fraction of the total discharge.

To evaluate this approximation, we now analyze top-view pictures of our developing fans (about 15 pictures per run). We first divide the surface of each fan into five concentric strips, where we count the active channels and measure their widths (at least two cross sections per channel, Fig. 10). We then average the number of channels and their width over runs. The resulting quantities depend on the time of their measurement, and on the distance to the apex, r. Further averaging over time yields radius-dependent quantities, whereas averaging over distance yields time-dependent quantities (Fig. 11).

When plotted as a function of radius, the width of the channels varies between about 1 and 2.5 cm, with no clear trend (Fig. 11a). The width variability is much larger in the proximal part of the fan than in its distal part. When plotted as a function of time, we find that the width is more consistent, with a relative variability of about 10% around a mean value of 1.3 cm (Fig. 11b). Overall, the channels appear reasonably homogeneous in size, suggesting that they share the total water discharge evenly.

The number of channels n_c varies between 5 and 6 across the fan (Fig. 11c). As expected for a radially oriented structure, we count fewer channels near the apex. We also find fewer channels near the toe, although the poor color contrast of the coal-dominated areas could bias our count. This variability compares with the disparity we observe between runs. The number of channels is nearly constant over time (Fig. 11d). Hereafter, we choose $n_c = 5.5$, and divide the total water discharge accordingly.

We now wish to compare the slope of our experimental fans with the threshold theory, applied to the characteristic channel defined above. This theory assumes that the combination of gravity and flow-induced shear stress maintains the channel bed at the threshold of motion (Glover and Florey, 1951; Henderson, 1961; Seizilles et al., 2013). As a result, the width, depth and slope of the channel are set by its water discharge. In particular, according to the simplest version of this theory (Devauchelle et al., 2011; Gaurav et al., 2015; Métivier et al., 2016b), the equilibrium slope reads

$$S_H = \left(g\,\mu^3\,\mathcal{L}^5\right)^{1/4} \sqrt{\frac{2^{3/2}\,\mathcal{K}(1/2) n_c}{3 C_f Q_w}}\,, \tag{9}$$

where μ is Coulomb's coefficient of friction (Table 1), $\nu = 10^{-6}$ m^{2}s^{-1} is the kinematic viscosity of water, $\mathcal{K}(1/2) \approx 1.85$ is the elliptic integral of the first kind, and C_f is Chézy's coefficient of fluid friction. The Chézy coefficient C_f depends on the bed roughness and the flow Reynolds number. For simplicity, we approximate it with a constant value of 0.02 (Moody, 1944; Ven Te, 1959). Finally, $\mathcal{L}$ is a characteristic length:

$$\mathcal{L} = \frac{\theta_c}{\mu}\,\frac{\rho_s - \rho}{\rho}\,d_s\,. \tag{10}$$

In our experiment, $\mathcal{L}$ is about $130\,\mu$m for silica and $65\,\mu$m for coal. Since we imposed the same water discharge during all experimental runs, and found the number of channels n_c to be relatively constant, the slope corresponding to the threshold theory depends on the sediment only. We find $S_{Hs} \approx 0.042$ for silica, and $S_{Hc} \approx 0.023$ for coal.

Intuitively, we expect the fan slope to increase with sediment discharge. Previous observations support this intuition, but there is no consensus yet about its physical origin, which involves the response of a single channel to sediment transport

Earth Surf. Dynam. Discuss., doi:10.5194/esurf-2016-56, 2016
Manuscript under review for journal Earth Surf. Dynam.
Published: 25 November 2016

and its destabilization into multiple threads (Whipple et al., 1998; Ashworth et al., 2004). We do not find any correlation between sediment discharge and slope in our experiment, despite considerable dispersion (Fig. 12). Even after normalizing our measurements according to the threshold theory, the data points appear segregated: the mean slope ratio of the silica deposit is about $S_s/S_{Hs} = 5.6 \pm 2.0$, whereas we find $S_c/S_{Hc} = 2.9 \pm 1.5$ for coal (this corresponds to $S_s \approx 0.23$ and $S_c \approx 0.068$). The silica deposit is steeper than the coal deposit, to a higher degree than predicted by the threshold theory. We have made an experimental fan with pure silica and the same water discharge to certify that the bimodal mixture does not cause the departure from threshold. The slope of this fan is also approximately five times higher than the threshold slope ($S_s = 0.2$). This is a common feature in experimental channels, as well as in natural rivers, although its origin is debated (Métivier et al., 2016a, b). A possible explanation is the infiltration of surface water into the sediment. Indeed, based on Eq. (9), a reduced water discharge induces a steeper channel. We were not able to measure the total water discharge near the fan toe, and therefore could not account for this leakage. Another likely cause for the channel steepening is sediment transport, which induces departure from threshold (Whipple et al., 1998; Guerit et al., 2014). Although we could not measure sediment discharge in the channels on our experimental fans, from visual observation it was clear that the sediment was in vigorous motion in the channels.

The slope ratio appears to be independent from the composition of the sediment mixture (Fig. 12). We can treat this observation as an empirical fact, and attribute a fixed value to the slope ratio: $\mathcal{S} = S_s/S_c = 3.4 \pm 1.0$. Substituting this value in Eqs. (7, 8), the mass balance of Sect. 5 relates, without any additional parameters, the composition of the sediment mixture to the location of the transition (Fig. 13). Despite significant uncertainties, our observations agree with this semi-empirical relationship. These uncertainties probably reflect the rudimentary mass balance we used.

7 Conclusion

Using a laboratory experiment, we generated alluvial fans fed with a bimodal sediment. The deposit they produce is segregated, with the less mobile sediment concentrated near the apex, and the more mobile one near the toe. This segregation also appears in the radial cross-section of the deposit in the form of a front that rises at a constant angle. The transition from the proximal deposit to the distal one occurs over about 30% of the total fan length, in the form of a complex stratigraphy. However, as a first approximation, we may represent this transition with a straight line, and treat the fan structure as two imbricated deposits. Combining this model with mass balance, we find that we can represent the self-similar growth of the fan with a precision of about 15%. This observation suggests that an alluvial fan acts essentially as a sieve, which segregates the sediment it is fed with. This process controls the geometry of the resulting deposit.

We expect this interpretation to hold for a richer mixture of sediments, although this assumption should be tested experimentally. The geometrical model we propose extends straightforwardly to an arbitrary number of grain sizes, and even to a continuous distribution. However, typical coarse alluvial fans, even though supplied with a wide range of grain sizes, often show a clear transition from gravel to sand over a front that we believe behaves similarly to the simplified fronts we observed in our experiments. As a consequence, we expect that the geometry of the final deposit (location and slope of the transition and proximal and distal slopes) allows us to estimate the relative flux that built the fan.

Earth Surf. Dynam. Discuss., doi:10.5194/esurf-2016-56, 2016
Manuscript under review for journal Earth Surf. Dynam.
Published: 25 November 2016

Our experiment suggests that the process by which an alluvial fan distributes grain sizes in its deposit, although a primary control on its structure, may not be the most puzzling component of its machinery. The way it selects its slope is a more challenging problem. Indeed, the threshold theory can only provide us with a first-order estimate of a channel slope, which proved underestimated by a factor of five in our experiments. Progress requires improvement in our understanding of how a channel reacts to sediment transport.

At least under some circumstances, a higher sediment discharge induces a steeper channel. Sometimes, like in our experiment, it also destabilizes the river into multiple channels, which then share water and sediment. In a fan, both mechanisms alter the slope of the deposit, and therefore its structure. To assess the influence of sediment discharge on channel slope, we need to either impose or measure its value. When the flow is distributed in multiple channels, measurement is the only way. Experimentally however, it is certainly easier to impose the sediment discharge of a single, stable channel.

Recent investigations have shown that, to keep a stable channel in a laboratory flume, we need to maintain the sediment discharge below a critical value (Seizilles et al., 2013; Métivier et al., 2016b). If this method works for a laboratory fan as well, it might produce simpler analogs of alluvial fans, and thus more convenient tools to investigate their formation.

Appendix A: Transport law

To calibrate the transport laws of our sediments, we use an independent set-up similar to that of Seizilles et al. (2014). The flow is confined between two Plexiglas panels separated by a 3.2 cm-wide gap in which we inject water and sediment at constant rate. Once the experiment has reached equilibrium, typically ten to twenty hours after it started, we measure the slope of the water surface S to estimate the shear stress τ. Since the Reynolds number is below 500 in our flume, we may assume that the flow is laminar. The shear stress acting on the sediment thus follows Poiseuille's law:

$$\tau = \rho (Sg)^{2/3} \left(\frac{3 Q_w \nu}{W} \right)^{1/3}, \tag{A1}$$

where W is the width of the gap. We then calculate the Shields parameter, which represents the ratio of the flow-induced shear stress τ to gravity:

$$\theta = \frac{\tau}{(\rho_s - \rho) g d_s}, \tag{A2}$$

and calibrate the transport law (Fig. 2). We find that below a critical value θ_c, which correspond to a critical shear stress τ_c, the sediment flux vanishes. Above this threshold, the flux appears proportional to the departure from the critical Shields parameter:

$$\frac{Q_s}{W} = q_0 (\theta - \theta_c), \tag{A3}$$

where q_0 = 28 $\pm$ 9 g s^{-1} m^{-1} and θ_c = 0.25 $\pm$ 0.02 for our silica grains, and q_0 = 77 $\pm$ 20 g s^{-1} m^{-1} and θ_c = 0.19 $\pm$ 0.008 for our coal grains.

Earth Surf. Dynam. Discuss., doi:10.5194/esurf-2016-56, 2016
Manuscript under review for journal Earth Surf. Dynam.
Published: 25 November 2016

Acknowledgements. We thank B. Erickson, E. Steen and C. Ellis for their help in building the experimental set-up; S. Harrington and K. François-King for assistance with experiments; J-L. Grimaud for the data on sediments; L. Guerit and E. Gayer for useful discussions.

Partial financial support was provided by US National Science Foundation grants 1242458 and 1246761. P.D. work at SAFL was funded by the grant of the Step'up doctoral school of IPGP and O.D. was funded by the *Émergence(s)* program of the *Mairie de Paris*, France.

Earth Surf. Dynam. Discuss., doi:10.5194/esurf-2016-56, 2016
Manuscript under review for journal Earth Surf. Dynam.
Published: 25 November 2016

References

Ashworth, P. J., Best, J. L., and Jones, M.: Relationship between sediment supply and avulsion frequency in braided rivers, Geology, 32, 21–24, 2004.

Blair, T. C. and McPherson, J. G.: Alluvial fans and their natural distinction from rivers based on morphology, hydraulic processes, sedimentary processes, and facies assemblages, Journal of sedimentary research, 64, 450–489, 1994.

Blissenbach, E.: Relation of surface angle distribution to particle size distribution on alluvial fans, Journal of Sedimentary Research, 22, 25–28, 1952.

Bryant, M., Falk, P., and Paola, C.: Experimental study of avulsion frequency and rate of deposition, Geology, 23, 365–368, 1995.

Bull, W. B.: The alluvial-fan environment, Progress in physical geography, 1, 222–270, 1977.

Charreau, J., Gumiaux, C., Avouac, J.-P., Augier, R., Chen, Y., Barrier, L., Gilder, S., Dominguez, S., Charles, N., and Wang, Q.: The Neogene Xiyu Formation, a diachronous prograding gravel wedge at front of the Tianshan: Climatic and tectonic implications, Earth and Planetary Science Letters, 287, 298–310, 2009.

Clarke, L., Quine, T. A., and Nicholas, A.: An experimental investigation of autogenic behaviour during alluvial fan evolution, Geomorphology, 115, 278–285, 2010.

Clarke, L. E.: Experimental alluvial fans: Advances in understanding of fan dynamics and processes, Geomorphology, 244, 135–145, 2015.

Clevis, Q., de Boer, P., and Wachter, M.: Numerical modelling of drainage basin evolution and three-dimensional alluvial fan stratigraphy, Sedimentary Geology, 163, 85–110, 2003.

Devauchelle, O., Petroff, A., Lobkovsky, A., and Rothman, D. H.: Longitudinal profile of channels cut by springs, Journal of Fluid Mechanics, 667, 38–47, 2011.

Drew, F.: Alluvial and lacustrine deposits and glacial records of the Upper-Indus Basin, Quarterly Journal of the Geological Society, 29, 441–471, 1873.

Dubille, M. and Lavé, J.: Rapid grain size coarsening at sandstone/conglomerate transition: similar expression in Himalayan modern rivers and Pliocene molasse deposits, Basin Research, 27, 26–42, 2015.

Einstein, H. A.: The bed-load function for sediment transportation in open channel flows, 1026, US Department of Agriculture, 1950.

Gaurav, K., Métivier, F., Devauchelle, O., Sinha, R., Chauvet, H., Houssais, M., and Bouquerel, H.: Morphology of the Kosi megafan channels, Earth Surface Dynamics, 3, 321, 2015.

Glover, R. E. and Florey, Q.: Stable channel profiles, US Department of the Interior, Bureau of Reclamation, Hydr. Lab. Report, 1951.

Guerit, L., Métivier, F., Devauchelle, O., Lajeunesse, E., and Barrier, L.: Laboratory alluvial fans in one dimension, Physical Review E, 90, 022 203, 2014.

Guerit, L., Barrier, L., Jolivet, M., Fu, B., and Métivier, F.: Denudation intensity and control in the Chinese Tian Shan: new constraints from mass balance on catchment-alluvial fan systems, Earth Surface Processes and Landforms, pp. 1088–1106, 2016.

Harvey, A. M., Mather, A. E., and Stokes, M.: Alluvial fans: geomorphology, sedimentology, dynamics—introduction. A review of alluvial-fan research, Geological Society, London, Special Publications, 251, 1–7, 2005.

Henderson, F. M.: Stability of alluvial channels, Journal of the Hydraulics Division, 87, 109–138, 1961.

Hinderer, M.: From gullies to mountain belts: a review of sediment budgets at various scales, Sedimentary Geology, 280, 21–59, 2012.

Houssais, M. and Lajeunesse, E.: Bedload transport of a bimodal sediment bed, Journal of Geophysical Research: Earth Surface, 117, (F4), 2012.

Jayko, A.: Late Quaternary denudation, Death and Panamint valleys, eastern California, Earth-Science Reviews, 73, 271–289, 2005.

Jolivet, M., Barrier, L., Dominguez, S., Guerit, L., Heilbronn, G., and Fu, B.: Unbalanced sediment budgets in the catchment–alluvial fan system of the Kuitun River (northern Tian Shan, China): Implications for mass-balance estimates, denudation and sedimentation rates in orogenic systems, Geomorphology, 214, 168–182, 2014.

Kiefer, E., Dorr, M. J., Ibbeken, H., and Gotze, H.-J.: Gravity-based mass balance of an alluvial fan giant: the Arcas Fan, Pampa del Tamarugal, Northern Chile, Andean Geology, 24, 165–185, 1997.

Le Hooke, R. B. and Rohrer, W. L.: Geometry of alluvial fans: Effect of discharge and sediment size, Earth Surface Processes, 4, 147–166, 1979.

Métivier, F., Devauchelle, O., Chauvet, H., Lajeunesse, E., Meunier, P., B., K., Ashmore, P., Zhang, Z., Fan, Y., and Liu, Y.: Geometry of meandering and braided gravel-bed threads from the Bayanbulak Grassland, Tianshan, PR China, Earth Surface Dynamics, 4, 273–283, 2016a.

Métivier, F., Lajeunesse, E., and Devauchelle, O.: Laboratory rivers: Lacey's law, threshold theory and channel stability, Submitted to Earth Surface Dynamics, 2016b.

Miller, K. L., Reitz, M. D., and Jerolmack, D. J.: Generalized sorting profile of alluvial fans, Geophysical Research Letters, 41, 7191–7199, 2014.

Moody, L. F.: Friction factors for pipe flow, Trans. Asme, 66, 671–684, 1944.

Paola, C., Heller, P. L., and Angevine, C. L.: The large-scale dynamics of grain-size variation in alluvial basins, 1: Theory, Basin Research, 4, 73–90, 1992a.

Paola, C., Parker, G., Seal, R., Sinha, S. K., Southard, J. B., and Wilcock, P. R.: Downstream fining by selective deposition in a laboratory flume, SCIENCE-NEW YORK THEN WASHINGTON-, 258, 1757–1757, 1992b.

Paola, C., Straub, K., Mohrig, D., and Reinhardt, L.: The "unreasonable effectiveness" of stratigraphic and geomorphic experiments, Earth-Science Reviews, 97, 1–43, 2009.

Parker, G.: Self-formed straight rivers with equilibrium banks and mobile bed. Part 2. The gravel river, Journal of Fluid Mechanics, 89, 127–146, 1978.

Parker, G.: Progress in the modeling of alluvial fans, Journal of Hydraulic Research, 37, 805–825, 1999.

Parker, G., Paola, C., Whipple, K. X., and Mohrig, D.: Alluvial fans formed by channelized fluvial and sheet flow. I: Theory, Journal of Hydraulic Engineering, 124, 985–995, 1998 a.

Parker, G., Paola, C., Whipple, K. X., Mohrig, D., Toro-Escobar, C. M., Halverson, M., and Skoglund, T. W.: Alluvial fans formed by channelized fluvial and sheet flow. II: Application, Journal of Hydraulic Engineering, 124, 996–1004, 1998 b.

Powell, E. J., Kim, W., and Muto, T.: Varying discharge controls on timescales of autogenic storage and release processes in fluvio-deltaic environments: Tank experiments, Journal of Geophysical Research: Earth Surface (2003–2012), 117, (F2), 2012.

Rachocki, A. and Church, M. A.: Alluvial fans: a field approach, John Wiley & Sons, 1990.

Reitz, M. D. and Jerolmack, D. J.: Experimental alluvial fan evolution: Channel dynamics, slope controls, and shoreline growth, Journal of Geophysical Research: Earth Surface (2003–2012), 117, 2012.

Reitz, M. D., Jerolmack, D. J., Lajeunesse, E., Limare, A., Devauchelle, O., and Métivier, F.: Diffusive evolution of experimental braided rivers, Physical Review E, 89, 052 809, 2014.

Rice, S.: The nature and controls on downstream fining within sedimentary links, Journal of Sedimentary Research, 69, 32–39, 1999.

Schumm, S. A., Mosley, M. P., and Weaver, W.: Experimental fluvial geomorphology, John Wiley and Sons Inc., New York, NY, 1987.

Earth Surf. Dynam. Discuss., doi:10.5194/esurf-2016-56, 2016
Manuscript under review for journal Earth Surf. Dynam.
Published: 25 November 2016

Seizilles, G., Devauchelle, O., Lajeunesse, E., and Métivier, F.: Width of laminar laboratory rivers, Physical Review E, 87, 052 204, 2013.

Seizilles, G., Lajeunesse, E., Devauchelle, O., and Bak, M.: Cross-stream diffusion in bedload transport, Physics of Fluids (1994-present), 26, 013 302, 2014.

Shields, A.: Anwendung der Ahnlichkeits Mechanik und der Turbulenz-forschung auf die Geschiebebewegung, Preussische Versuchsanstalt fur Wasserbau und Schiffbau, 26, 524–526, 1936.

Sinha, R.: The Great avulsion of Kosi on 18 August 2008., Current Science (00113891), 97, 2009.

Slingerland, R. and Smith, N. D.: River avulsions and their deposits, Annu. Rev. Earth Planet. Sci., 32, 257–285, 2004.

Smith, G. H. S. and Ferguson, R. I.: The gravel-sand transition: flume study of channel response to reduced slope, Geomorphology, 16, 147–159, 1996.

Stebbings, J.: The shapes of self-formed model alluvial channels., Proceedings of the Institution of Civil Engineers, 25, 485–510, 1963.

Stock, J. D., Schmidt, K. M., and Miller, D. M.: Controls on alluvial fan long-profiles, Geological Society of America Bulletin, 120, 619–640, 2008.

Van Dijk, M., Postma, G., and Kleinhans, M. G.: Autocyclic behaviour of fan deltas: an analogue experimental study, Sedimentology, 56, 1569–1589, 2009.

Ven Te, C.: Open channel hydraulics, 1959.

Viparelli, E., Solari, L., and Hill, K.: Downstream lightening and upward heavying: Experiments with sediments differing in density, Sedimentology, 62, 1384–1407, 2015.

Whipple, K. X., Parker, G., Paola, C., and Mohrig, D.: Channel dynamics, sediment transport, and the slope of alluvial fans: Experimental study, The Journal of geology, 106, 677–694, 1998.

Whittaker, A. C., Duller, R. A., Springett, J., Smithells, R. A., Whitchurch, A. L., and Allen, P. A.: Decoding downstream trends in stratigraphic grain size as a function of tectonic subsidence and sediment supply, Geological Society of America Bulletin, 123, 1363–1382, 2011.

Wilcock, P. R. and Crowe, J. C.: Surface-based transport model for mixed-size sediment, Journal of Hydraulic Engineering, 129, 120–128, 2003.

Earth Surf. Dynam. Discuss., doi:10.5194/esurf-2016-56, 2016
Manuscript under review for journal Earth Surf. Dynam.
Published: 25 November 2016

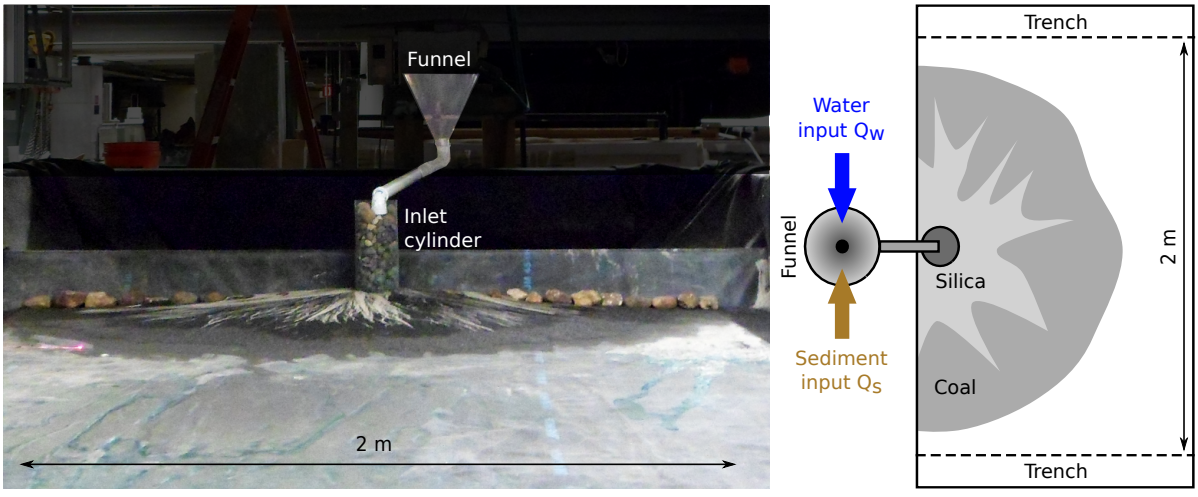

Figure 1. Experimental set-up. Left: front-view picture. Right: top-view representation.

Table 1. Physical characteristics of the sediment. Measurement method is presented in Appendix A.

	Density	Grain size	
	ρ_s (kg m^{-3})	d_{50} (μm)	d_{90} (μm)
Silica	2650 ± 50	130	200
Coal	1500 ± 50	400	800

	Critical Shields	Friction coefficient
	θ_c	μ
Silica	0.25 ± 0.02	0.42 ± 0.04
Coal	0.19 ± 0.008	0.58 ± 0.04

Table 2. Experimental parameters for the five runs.

Run	Water discharge	Sediment discharge	Silica fraction
	Q_w (L min^{-1})	Q_s (g min^{-1})	ϕ
1	2.6 ± 0.1	89 ± 5	0.5±0.05
2	2.6 ± 0.1	200 ± 5	0.5±0.05
3	2.6 ± 0.5	105 ± 5	0.25±0.02
4	2.4 ± 0.1	105 ± 5	0.25±0.02
5	2.6 ± 0.1	105 ± 5	0.8±0.08

Earth Surf. Dynam. Discuss., doi:10.5194/esurf-2016-56, 2016
Manuscript under review for journal Earth Surf. Dynam.
Published: 25 November 2016

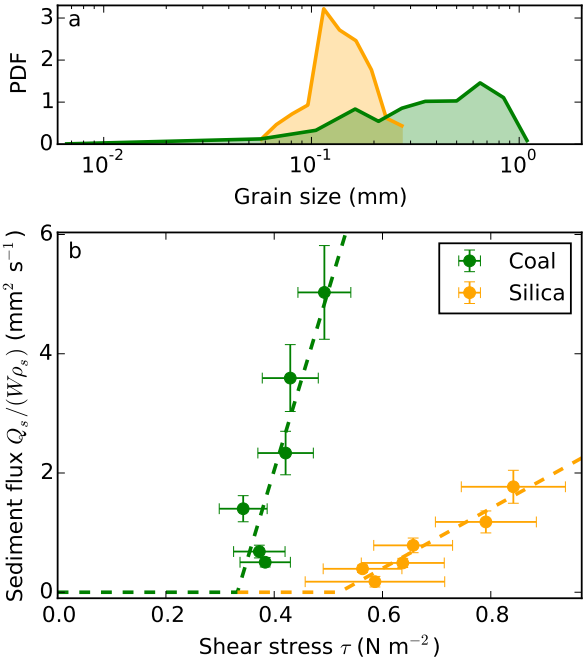

Figure 2. (a) Probability density function of the grain size. Orange: silica, green: coal. (b) Transport laws. Volumetric flux per unit width, as a function of dimensional shear stress. Dashed lines correspond to Eq. (A3) fitted to the data (method in Appendix A, coefficients in Table 1).

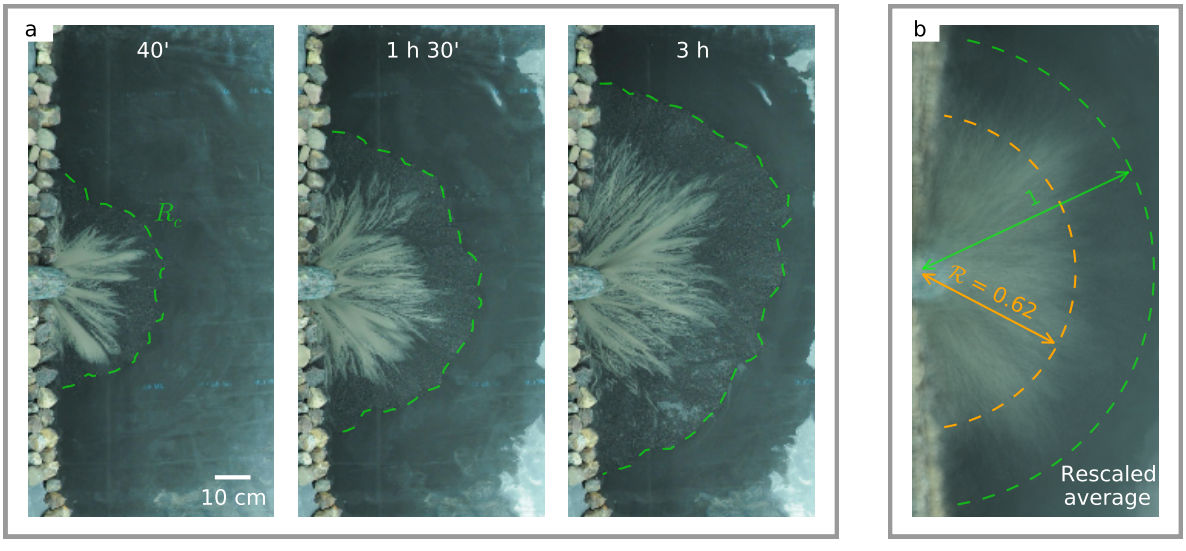

Figure 3. Top-view pictures of an experimental fan (run 2). (a) Time evolution. Green dashed line indicates fan toe, R_c. (b) Average of rescaled pictures. The 26 pictures are 10-minutes apart. Dashed lines indicate silica-coal transition (orange) and fan toe (green). After rescaling, the fan length is one. Transition between silica and coal occurs at dimensionless distance $\mathcal{R}$ from apex.

Earth Surf. Dynam. Discuss., doi:10.5194/esurf-2016-56, 2016
Manuscript under review for journal Earth Surf. Dynam.
Published: 25 November 2016

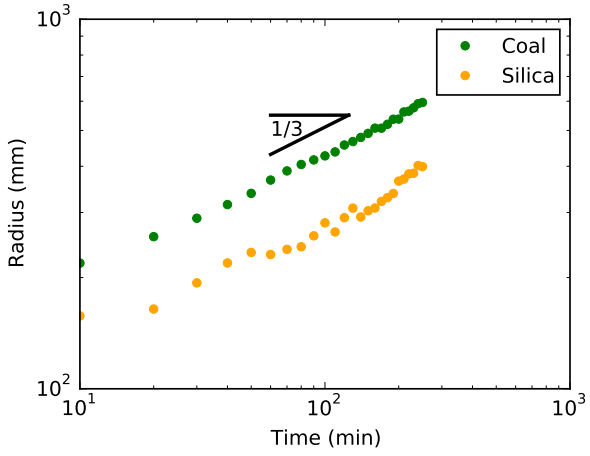

Figure 4. Evolution of silica (orange) and coal (green) radii during run 2.

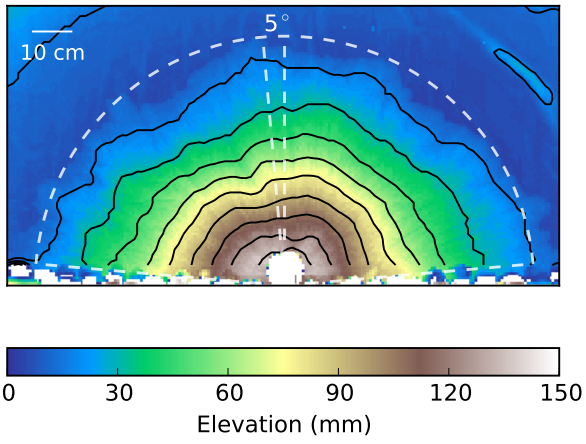

Figure 5. Topography of an experimental fan (run 2). Black lines: elevation contours 15 mm apart from each other. White dashed lines indicate the bounds used for averaging (only two radii appart from 5° are represented for clarity).

Table 3. Geometrical characteristics of the experimental fans.

Run	Slope ratio $\mathcal{S}$	Transition location $\mathcal{R}$	S_t/S_s $\mathcal{S}_t$
1	3 ± 0.3	0.56 ± 0.07	0.37 ± 0.08
2	2.9 ± 0.1	0.55 ± 0.09	0.36 ± 0.08
3	4 ± 0.6	0.41 ± 0.1	0.57 ± 0.12
4	4.6 ± 0.6	0.39 ± 0.1	0.61 ± 0.13
5	3.3 ± 0.3	0.83 ± 0.2	0.12 ± 0.03

Earth Surf. Dynam. Discuss., doi:10.5194/esurf-2016-56, 2016
Manuscript under review for journal Earth Surf. Dynam.
Published: 25 November 2016

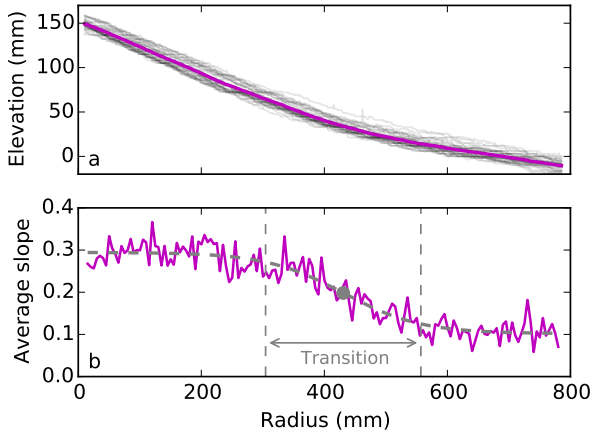

Figure 6. (a) Fan profiles at different angles (run 2). Gray: individual profiles; magenta: average profile. (b) Average downstream slope (magenta). Fitted hyperbolic tangent (dashed gray). Inflection point (gray dot) and boundary of the transition area (vertical dashed gray line).

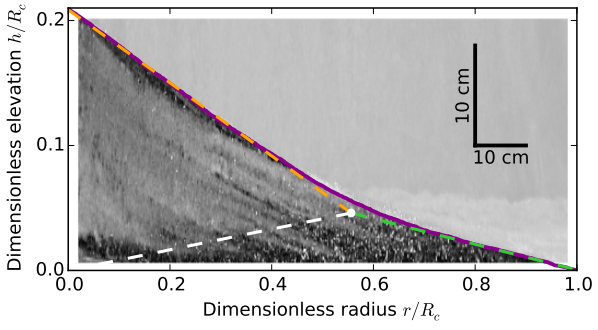

Figure 7. Average radial profile (magenta line), superimposed on radial cross section. Dashed lines: slope of the silica (orange) and coal (green) deposits. White dashed line indicates silica-coal transition. Scale is for the picture. h and r are respectively the fan elevation and the distance to the apex.

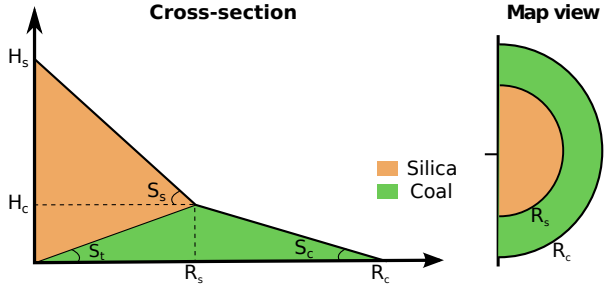

Figure 8. Representation of an alluvial fan (template). Silica: orange; coal : green.

Earth Surf. Dynam. Discuss., doi:10.5194/esurf-2016-56, 2016
Manuscript under review for journal Earth Surf. Dynam.
Published: 25 November 2016

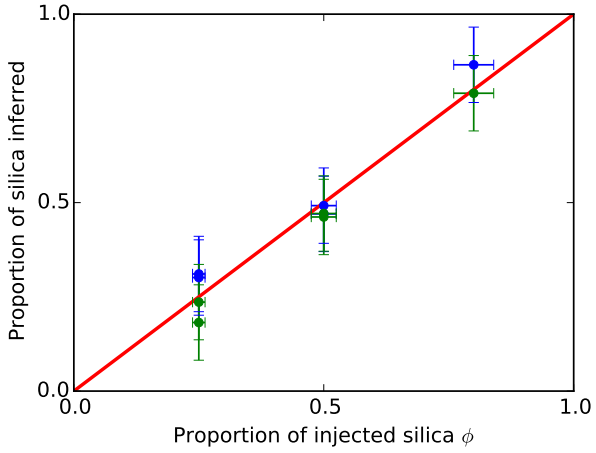

Figure 9. Proportion of silica inferred from the geometry of the deposit, after Eq. (7) (blue) and after Eq. (8) (green), as a function of the composition of the sediment input. Red line: perfect agreement.

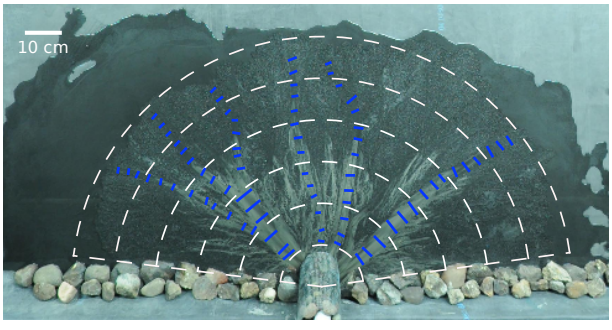

Figure 10. Top-view of an experimental fan superimposed with measurement strips (white), and channels cross-sections (blue).

Earth Surf. Dynam. Discuss., doi:10.5194/esurf-2016-56, 2016
Manuscript under review for journal Earth Surf. Dynam.
Published: 25 November 2016

Earth Surface Dynamics Discussions
Open Access
EGU

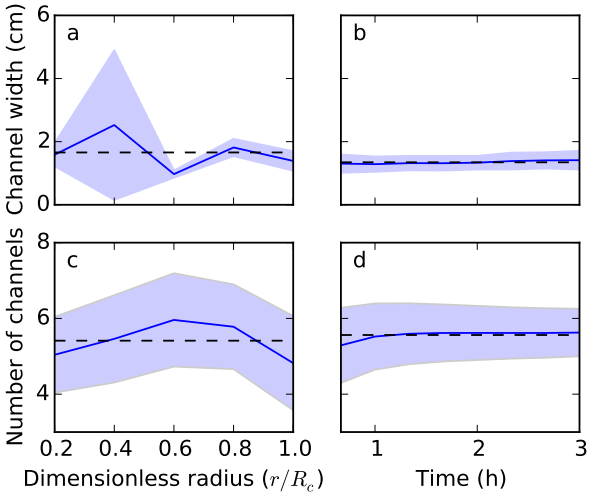

Figure 11. Evolution of active channels for all the runs. Channel width as a function of the dimensionless radius (a) and time (b). Number of channels as a function of dimensionless radius (c) and time (d). Black dashed line: average. Shaded area: variability over experimental runs.

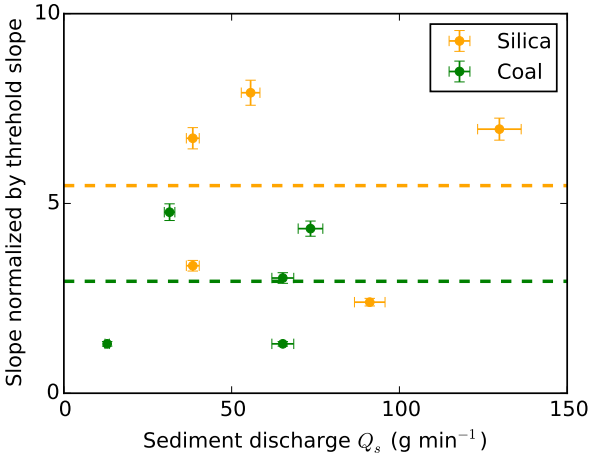

Figure 12. Slope normalized by the threshold slope, calculated with Eq. (9), as a function of the sediment discharge. Dashed lines: average slopes.

Earth Surf. Dynam. Discuss., doi:10.5194/esurf-2016-56, 2016
Manuscript under review for journal Earth Surf. Dynam.
Published: 25 November 2016

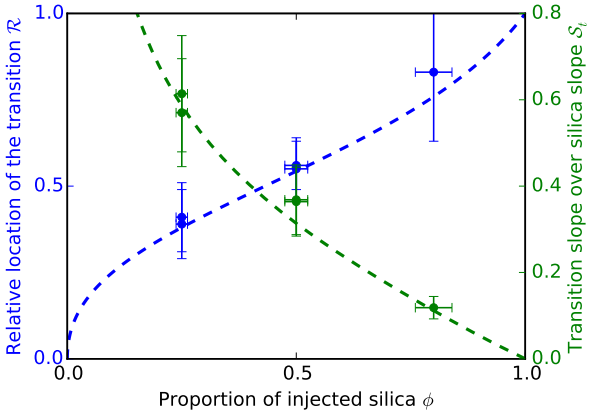

Figure 13. Relative position of the transition $\mathcal{R}$ (blue) and dimensionless transition slope $\mathcal{S}_t$ (green), as a function of the composition of the sediment input. Dot: experimental measurements. Dashed line: Eqs. (7, 8) with $\mathcal{S} = 3.4$.